Efficiency of multi-beam Fourier phase gratings at 1.4 THz

Mirzaei, B.; Silva, J. R.G.; Luo, Y.; Liu, X. X.; Wei, L.; Hayton, Darren J.; Gao, J. R.; Groppi, C

DOI
10.1364/OE.25.006581

Publication date
2017

Document Version
Final published version

Published in
Optics Express

Research Article | Vol. 25, No. 6 | 20 Mar 2017 | OPTICS EXPRESS 6581

Optics EXPRESS

Efficiency of multi-beam Fourier phase gratings at 1.4 THz

B. MIRZAEI,[1,6] J. R. G. SILVA,[2] Y. C. LUO,[1] X. X. LIU,[3] L. WEI,[4] D. J. HAYTON,[2] J. R. GAO,[1,2,7] AND C. GROPPI[5]

[1]*Kavli Institute of NanoScience, Delft University of Technology, Delft, Netherlands*
[2]*SRON Netherlands Institute for Space Research, Groningen/Utrecht, Netherlands*
[3]*Microelectronics Department, Delft University of Technology, Delft, Netherlands*
[4]*Imaging Physics Department, Delft University of Technology, Delft, Netherlands*
[5]*School of Earth and Space Exploration, Arizona State University, AZ, USA*
[6]*b.mirzaei@tudelft.nl*
[7]*j.r.gao@tudelft.nl*

Abstract: We compare the results of simulated and measured power efficiency and far-field beam pattern, for two reflective Fourier phase gratings, designed to generate 2 × 2 and 2 × 4 beams respectively from a single-beam, coherent source at 1.4 THz. The designed surface structures were manufactured on aluminum plates by a computer numerical control (CNC) micro-milling machine. Despite small differences between the designed and fabricated gratings, we measured power efficiencies of both gratings to be around 70%, which is in a good agreement with the simulated values. We also find a good agreement between the simulated and measured diffracted beam size and spatial distribution. We demonstrate the application of both gratings as multiple beam local oscillators to simultaneously pump (or operate) a 4-pixel array of superconducting heterodyne mixers.

OCIS codes: (050.1950) Diffraction gratings; (040.2840) Heterodyne; (040.2235) Far infrared or terahertz; (040.1240) Arrays; (350.1260) Astronomical optics.

References and links

1. W. Zhang, P. Khosropanah, J. R. Gao, E. L. Kollberg, K. S. Yngvesson, T. Bansal, R. Barends, and T. M. Klapwijk, "Quantum noise in a terahertz hot electron bolometer mixer," Appl. Phys. Lett. **96**(11), 111113 (2010).
2. B. D. Jackson, A. M. Baryshev, G. de Lange, J. R. Gao, S. V. Shitov, N. N. Iosad, and T. M. Klapwijk, "Low-noise 1 THz superconductor–insulator–superconductor mixer incorporating a NbTiN/SiO2/AlNbTiN/SiO2/Al tuning circuit," Appl. Phys. Lett. **79**(3), 436–438 (2001).
3. C. Walker, *Terahertz Astronomy* (CRC, Taylor & Francis Group, 2016), Chap. 5&6.
4. J. A. Murphy, C. O'Sullivan, N. Trappe, W. Lanigan, R. Colgan, and S. Withington, "Modal Analysis of the Quasi-Optical Performance of Phase Gratings," Int. J. Inf. Mill. Waves **20**(8), 1469–1486 (1999).
5. U. U. Graf, and S. Heyminck, "Fourier gratings as submillimeter beam splitters," IEEE Trans. Antenn. Propag. **49**(4), 542–546 (2001).
6. W. Lanigan, N. Trappe, J. A. Murphy, R. Colgan, C. O'Sullivan, and S. Withington, "Quasi-optical multiplexing using reflection phase gratings," in *Proceedings of the 11th International Symposium on Space Terahertz Technology* (University of Michigan, 2000), pp. 616–625.
7. C. E. Groppi, C. K. Walker, C. Kulesa, D. Golish, A. Hedden, P. Gensheimer, G. Narayanan, A. W. Lichtenberger, U. U. Graf, and S. Heyminck, "Desert STAR: A 7 pixel 345 GHz heterodyne array receiver for the Heinrich Hertz Telescope," Proc. SPIE **4855**, 330–337 (2003).
8. S. Heyminck, and U. U. Graf, "Reflection gratings as THz local oscillator multiplexer," Proc. SPIE **4014**, 164–171 (2000).
9. U. U. Graf, S. Heyminck, E. A. Michael, S. Stanko, C. E. Honingh, K. Jacobs, R. T. Schieder, J. Stutzki, and B. Vowinkel, "SMART: the KOSMA sub-millimeter array receiver for two frequencies," in *Proceedings of the 13th International Symposium on Space Terahertz Technology* (Harvard University, 2002), pp. 143–152.
10. N. Hurtado, U. U. Graf, H. Adams, C. E. Honingh, K. Jacobs, P. Pütz, R. Güsten, and J. Stutzki, "Optics and cryogenics for the 1.1 THz multi-pixel heterodyne receiver for APEX," Proc. SPIE **9153**, 915327 (2014).
11. C. Risacher, R. Güsten, J. Stutzki, H. W. Hübers, D. Büchel, U. U. Graf, S. Heyminck, C. E. Honingh, K. Jacobs, B. Klein, T. Klein, C. Leinz, P. Pütz, N. Reyes, O. Ricken, H. J. Wunsch, P. Fusco, and S. Rosner, "First Supra-THz Heterodyne Array Receivers for Astronomy With the SOFIA Observatory," IEEE Trans. Terahertz Sci. Technol. **6**(2), 199–211 (2016).

#285910 https://doi.org/10.1364/OE.25.006581
Journal © 2017 Received 30 Jan 2017; revised 5 Mar 2017; accepted 9 Mar 2017; published 13 Mar 2017

Optics EXPRESS

12. C. Groppi, C. Walker, C. Kulesa, D. Golish, J. Kloosterman, S. Weinreb, G. Jones, J. Barden, H. Mani, T. Kuiper, J. Kooi, A. Lichtenberger, T. Cecil, and G. Narayanan, P. Puˈtz and A. Hedden, "SuperCam: A 64 pixel heterodyne array receiver for the 350 GHz atmospheric window," in *Proceedings of the 20th International Symposium on Space Terahertz Technology* (Charlottesville, 2009), pp. 90–96.
13. J. V. Siles, R. H. Lin, C. Lee, E. Schlecht, A. Maestrini, P. Bruneau, A. Peralta, J. Kloosterman, J. Kawamura, and I. Mehdi, "Development of High-Power Multi-Pixel LO Sources at 1.47 THz and 1.9 THz for Astrophysics: Present and Future," in *Proceedings of the 26th International Symposium on Space Terahertz Technology* (Cambridge, MA, 2015), pp. 40–42.
14. B. S. Williams, "Terahertz quantum-cascade lasers," Nat. Photonics **1**(9), 517–525 (2007).
15. Y. C. Luo, X. X. Liu, D. J. Hayton, L. Wei, J. R. Gao, and C. Groppi, "Fourier phase grating for THz multi-beam local oscillators," in *Proceedings of the 26th International Symposium on Space Terahertz Technology* (Cambridge, MA, 2015), pp. 77–78.
16. H. Dammann, and E. Klotz, "Coherent optical generation and inspection of two-dimensional periodic structures," Int. J. Opt. **24**(4), 505–515 (1977).
17. H. Ehrenreich, H. R. Philipp, and B. Segall, "Optical properties of aluminum," Phys. Rev. **132**(5), 1918–1928 (1963).
18. W. D. Furlan, V. Ferrando, J. A. Monsoriu, P. Zagrajek, E. Czerwińska, and M. Szustakowski, "3D printed diffractive terahertz lenses," Opt. Lett. **41**(8), 1748–1751 (2016).
19. H. Ekström, B. S. Karasik, E. Kollberg, and K. S. Yngvesson, "Conversion gain and noise of niobium superconducting hot-electron-mixers," IEEE Trans. Microw. Theory Tech. **43**(4), 938–947 (1995).

1. Introduction

Terahertz heterodyne receivers, typically consisting of a superconducting mixer and a coherent local oscillator (LO) source, are approaching quantum-noise limited sensitivity [1,2]. Therefore, to further improve spatial observing efficiency, multi-pixel heterodyne receivers [3] are necessary, in particular, for sky mapping from astronomical telescopes. Historically, the utilization of large, multi-pixel heterodyne arrays has been held back by the cost and high complexity of multi-beam, frequency or phase matched, local oscillators. One approach is to generate multiple beams from a single beam source by manipulation of its phase by means of a phase grating [4,5]. Considering the challenges in providing suitable THz sources and complexities to synchronize the frequency or phase of many individual sources, this approach is more favourable and practical than providing each pixel with a separate LO. For the application of such a grating, a key figure of merit when converting a single beam into multiple beams is the power efficiency of the conversion, that is, the ratio between the total power of the resulting multiple beams and that of the input single beam.

A phase grating consists of a periodic structure made up of unit cells whereby each cell modulates the phase of the incident electro-magnetic wave in order to produce a series of diffraction orders with different traveling angles. The intensity and angular distribution of the diffraction orders are determined by the unit cell modulation pattern and size. To effectively match the beam pattern to that of a mixer array, additional optics, such as a parabolic mirror or lens, is typically needed for both properly collimating the diffracted beams and controlling spatial distribution.

Since the first grating design for 90-110 GHz [6], several milestones have been reached towards developing THz phase gratings. Sorting by the operating frequency, the following phase gratings have been reported: 7-pixel grating at 345 GHz has been realized with 80% efficiency [7], 8-pixel grating at 500 GHz with 83% efficiency [8], 8-pixel grating at 490 & 810 GHz [9] and 3-pixel grating at 1.1 THz [10]. Beyond these frequencies, little work can be found in the literature. Although a 7-pixel grating at 1.9 THz has been reported [11] no information on the grating measurements and analysis has been given.

Although waveguide based multiple beam generators [12,13] may provide high efficiency, very few experiments are found in the literature. Furthermore, manufacturing of the waveguides, in particular, at the supra-THz frequency range (>1 THz), such as the frequency band centered at 4.7 THz, which is significant for astronomical applications, becomes increasing difficult and costly. Moreover, this approach has also difficulties to make use of existing sources, such as quantum cascade lasers [14]. Therefore, we choose to develop a phase grating, namely with a quasi-optical coupling to a mixer array approach in contrast to

Optics EXPRESS

the waveguide approach. In this work we present two different phase gratings of 4 and 8-pixels, designed to operate at 1.4 THz. This frequency was chosen because of the availability of a high power gas laser source, facilitating the experimental study of the grating with the goal of improving understanding of the performance, namely the efficiency and the spatial distribution of diffracted beams by comparing the simulations with measurements.

2. Fourier Phase Gratings, design and manufacturing

In a Fourier phase grating, the surface topology of a unit cell is derived based on a Fourier series with a certain number of coefficients. Increasing this number in the design makes the calculated surface structure closer to the ideal, leading to greater power efficiency. However, to balance accuracy of the end result with increasing computation demand, we typically limit the calculation to 13 Fourier coefficients to design our gratings, which ensure at least 98% of the maximum achievable efficiency if an infinite number of coefficients were to be used [5]. Having built a proper algorithm in MATLAB, we find 13 coefficients to satisfy the following condition for 2 and 4 diffraction orders in one dimension (1D), respectively: $\sum_{i=\pm1}(p_i-\frac{1}{2})^2<0.01$ and $\sum_{i=\pm1,\pm3}(p_i-\frac{1}{4})^2<0.01$, where p_i is the fractional power of the i'th diffraction order. By minimizing these summations, we come up with final selected coefficients. The 2D surface profile of a unit cell is then generated by superimposing two sets of such 1D Fourier coefficients orthogonally. Therefore, the power efficiency is calculated by the product of summation of all fractional powers in both directions.

The divergence of the diffracted beams is inversely proportional to the unit cell size. The direction of each diffraction order can be calculated by the expression, $\sin\beta = \sin\alpha + m\lambda/\Lambda$, where Λ is the side length of the square unit cells, which also defines the periodicity of the grating, α and β are the angles of incidence and the m'th diffraction order, respectively. Both angles are with respect to the normal incidence on the grating. In this work, we chose a unit cell with an area of 2 × 2 mm^2 (Λ = 2 mm) to reach a suitable angular distribution of the diffracted beams, to be measurable with available experimental setup, and also for later matching a mixer array. Figure 1 shows the surface profiles of unit cells in 3D, designed for 4 (2 × 2) and 8 (2 × 4)-pixel gratings which are repeated 15 times in two orthogonal directions to form the gratings with a total area of 30 × 30 mm^2. We note that the design of the 4-pixel grating and the initial measurements have been reported by us previously in [15].

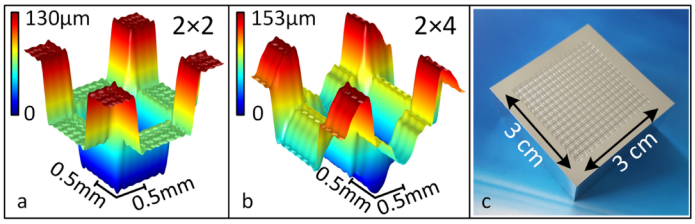

Fig. 1. 3D surface profiles of unit cells of 4 (a) and 8-pixel (b) gratings with exaggerated z axis and a photograph of the manufactured 8-pixel grating (c).

Unlike traditional Dammann gratings with sharp step like variations in the surface structure [16], the smooth and continuous surface of the Fourier phase gratings can be accurately machined on a metallic plate to make a reflection grating. A KERN EVO micro-milling machine with a ball end mill is used to transfer the designed pattern onto aluminum, which is expected to have more than 99% surface reflectivity at THz frequencies [17]. A micrograph of the manufactured 8-pixel grating is also shown in Fig. 1. The manufacturing accuracy is limited by the radius of the ball end-mill machine tool, which defines the minimum radius of curvature that can be patterned. Ideally, the latter should match to the designed value. In practice, the minimum radius of curvature becomes smaller with a larger

Optics EXPRESS

number of Fourier coefficients, i.e. appearance of finer-scale variation with smaller unit cell size, i.e. lateral compression of the profile and also with longer operating wavelength requiring greater profile depth. The minimum radius of curvature of our 4 and 8-pixel grating designs are 122 and 106 μm, respectively. In contrast, the smallest available radius of the diamond ball end-mill used is only 300 μm. Therefore, we do not expect the designed profile to be fully reproduced in manufacturing. Figure 2 shows two cross sections or surface profiles measured orthogonally from a unit cell of the manufactured 8-pixel grating, together with the designed profiles, for comparison. Although there are some small deviations, less than 3 μm in amplitude, the main topology is reasonably realized. An alternative manufacturing route is the 3D printing [18] technique, which has been successfully applied for the THz plastic lenses. The expected challenge is the material, which has to be a highly conductive metal, such as pure Al with extremely fine structure.

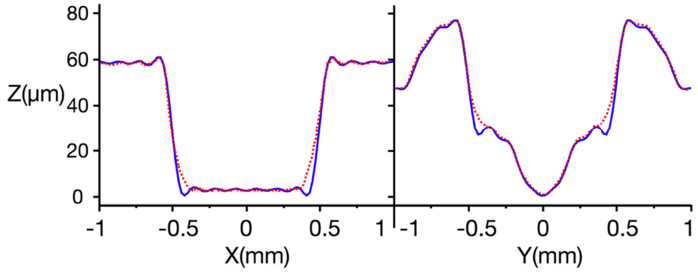

Fig. 2. Two cross sections or surface profiles measured orthogonally from a unit cell of the manufactured 8-pixel grating (dashed), together with the designed profiles (solid), for comparison (corresponding to the 3D profile shown in the middle of the Fig. 1). Here Z is the vertical direction of the grating.

3. Simulation and measurement results

We use the RF module of COMSOL to fully simulate the 3D performance of the designed gratings in order to compare with the measured results. To calculate the efficiency, we input the surface morphology of a unit cell into the model and apply periodic port and boundary conditions to simulate the entire grating. There we can derive the direction and configuration of the diffracted beams as well as the power fraction of each individual order and the total grating power efficiency. However, this approach does not produce the far-field beam pattern. In order to do so, we model the entire grating by repeating the unit cell geometry in both orthogonal directions. Although this demands more processing time (30 versus 15 minutes), the advantage of this approach is that we are able to perform the simulation using the same parameters as in the experiment, i.e. the shape of the incoming beam and the number of illuminated unit cells. In practice, we apply five processors of 2.5 GHz, each with a memory of 6.4 Gb.

Figure 3 illustrates the measurement setup used to characterize the 8-pixel grating. We use a far infrared (FIR) gas laser operating at 1.4 THz to generate the incoming beam to the grating. The laser beam illuminates the grating through a focusing lens (with 250 mm focal distance) and with an incident angle of θ. The incident beam pattern mapped at the equivalent position of the grating is depicted in Fig. 4(f), where it can be seen that the beam has a non-uniform intensity distribution, characterized with two peaks, originated from the output of the gas laser, with an area covering about 12 unit cells on the grating.

Optics EXPRESS

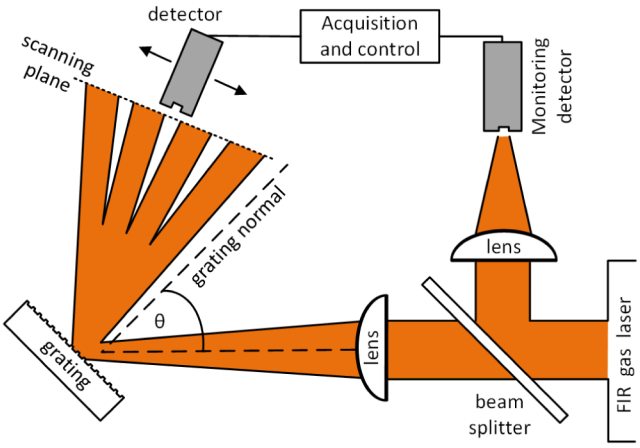

Fig. 3. Schematic view of the experimental setup for measuring the beam patterns diffracted from the grating.

We measure the output beams diffracted by the grating by scanning a pyro-electric detector, mounted on a X-Y motor controlled translation stage. The scanning plane is 60 mm away from the grating and is normal to the imaginary line drawn from the centre of the grating to the centre of the beam pattern, ensuring symmetric results. The lens is chosen as such to produce a focal point at the scanning plane, giving cleaner measured diffracted beams. Because the entrance aperture of the pyro-electric detector is 2 mm in diameter, we choose 1 mm as the scanning step size to effectively scan the whole target area. Since the output power of the gas laser fluctuates in time, we introduce a beam splitter and an additional pyro-electric detector to monitor the instantaneous power as reference to correct the fluctuations in the acquired diffracted beam pattern.

We repeat the measurement for two different incident beams with orthogonal azimuth angles, by 90° rotation of the grating on the fixed plane. To distinguish these two cases, we show the arrows schematically to represent the diffracted beams, each with a different colour, as well as the incident beam in red, in the Figs. 4(a) and 4(b), which are the results from the 3D simulations in COMSOL. The measurement results for the case of $\theta = 25°$ are plotted in the left side of Figs. 4(c) and 4(d), corresponding to the cases shown in Figs. 4(a) and 4(b), respectively. We find that in the first case (Fig. 4(c)) the power is more uniformly distributed among the diffracted beams, which are symmetrically distributed in space, making it more favorable for the application as local oscillator for a mixer array. For comparison, the simulation results are plotted next to the measured results in Figs. 4(c) and 4(d), where they show a good agreement in terms of the diffracted beam distribution and the size of the beam pattern. The cause of the different beam patterns produced by different applied incident beams is the unit cell profile asymmetry of the 8-pixel grating. In fact, the projection of the incident beam on the grating surface is perpendicular to 1×2 (Fig. 2 left) for the first incident beam and to 1×4 (Fig. 2 right) grating 1D profile for the second incident beam. It is worth mentioning that in the simulation, we take the same size as the experimental incident beam, but with a single Gaussian-like profile instead of the double peaked beam produced by the gas laser. Because of this, the simulation does not reproduce the exact shape of the experimental diffracted beams.

Since the beam patterns are measured along a flat, not a spherical plane, they look slightly distorted and stretched. For clarity, the simulated beam pattern in Fig. 4(c), is plotted on a spherical surface and included in Fig. 4(e), which illustrates clearly that the beams are actually distributed in straight rows and columns.

Optics EXPRESS

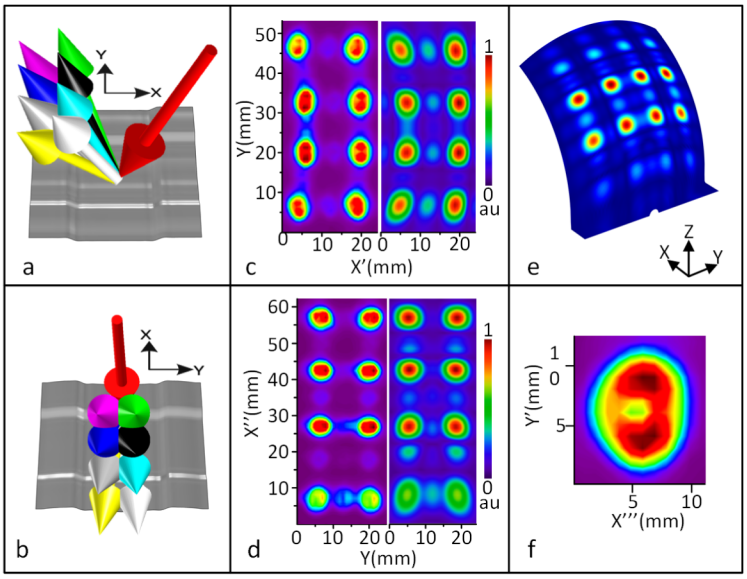

Fig. 4. (a,b) Arrow schematics illustrate the simulation results of diffraction orders, corresponding to two incident beams with 90° azimuth angle difference on the 8-pixel grating; (c,d) Planar measured (left) and simulated (right) far-field beam patterns at 60 mm from the grating with incident beams corresponding to (a) and (b) respectively; (e) the simulated far-field beam pattern of the case corresponding to (a) shown on a spherical surface; (f) Measured incident beam on the grating.

To obtain the efficiency experimentally, we integrate the measured intensity of all 8 beams, excluding other orders, and divide it by the integrated intensity of the incoming beam at the grating position. Taking the air absorption in the optical path between the grating and the scanning plane into account, we end up with a measured efficiency of 73 ± 1%. The 2% uncertainty originates from both the air loss estimation and the background noise of the pyro-electric (room temperature) detector. Comparing to the expected values of 73.8% from the 3D COMSOL simulations and 72% from the Fourier series calculation in the design, for the same incident angle ($\theta = 25°$), we conclude that the measured efficiency is in good agreement with that predicted by the simulations.

An interesting question is: how much does the deviation of the manufactured grating surface structure from the design affect the efficiency? For this, we perform the simulation, by taking the measured grating surface profile as the input to the 3D COMSOL, where we find a drop of about 0.3% in the efficiency and a negligible difference in the beam pattern, calculated using the designed surface profile. Taking advantage of this capability in COMSOL simulations, allows us to conclude for the first time that, even with non-ideal machining, one can reach nearly the theoretically predicted efficiency and beam pattern. This conclusion has a high impact on the manufacturability of a grating, making its fabrication less critical.

We also study the effect of different incident angles θ on the far-field angular and power distributions of the diffracted beams and on the grating power efficiency, for the case corresponding to Fig. 4(a). The simulation results are plotted in Fig. 5 for four incident angles of 15°, 20°, 25° and 30°, where each sub-figure contains the azimuth angle and the elevation angle with respect to the grating surface, together with the power fraction of all diffracted beams that are separated by circles filled by different colours, corresponding to the arrows in Fig. 4(a). This figure shows that by increasing the angle with respect to the normal incidence, the power distribution becomes less uniform whilst the power efficiency decreases negligibly by less than 2%.

Optics EXPRESS

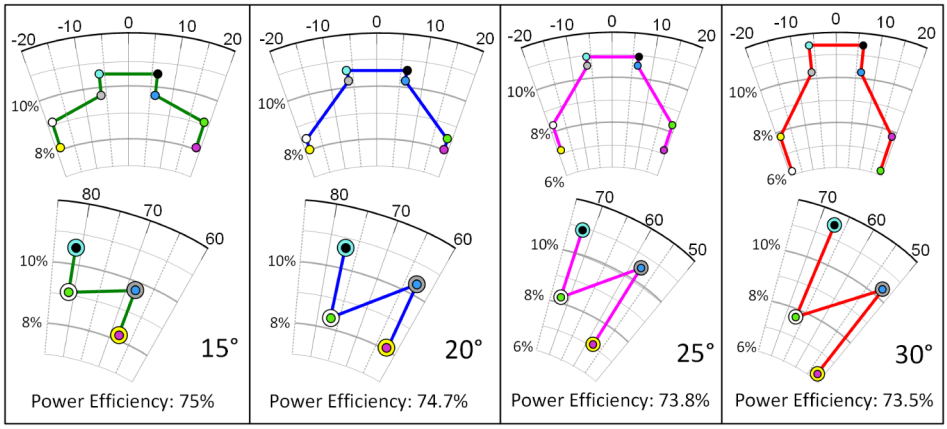

Fig. 5. Angular and power distributions of diffracted beams for the case shown in Fig. 4(a), for four different incident angles. The power fractions in the top and bottom plots of each section are shown versus the azimuth angle and the elevation angle with respect to the grating surface, for different diffracted orders, respectively. Each diffraction order is distinguished by the colour of the corresponding arrow in Fig. 4(a). In the elevation angle plots, the doubled circles indicate the overlapping of two corresponding diffracted beams.

We apply a similar measurement setup, to characterize the beam pattern of the 4-pixel grating. Figure 6 shows the measured incident beam on the grating with θ = 25°, and also the measured and simulated diffracted beams, both of which are at a plane, being 12 cm away from the grating. Very similar overall beam shapes and sizes show a high correlation between the measurements and simulations. All diffracted beams actually duplicate the detailed profile of the incident beam.

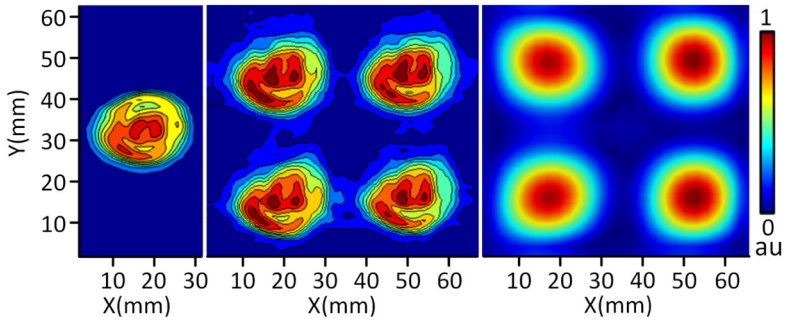

Fig. 6. Measured incident beam (right) and measured (middle) and simulated (right) diffracted beam patterns of the 4-pixel grating at a plane, which is 12 cm away from the grating. Small differences in the measured beam profiles are likely due to the FIR laser, the profile of which is found to vary in time.

To derive the efficiency of the 4-pixel grating, we apply a slightly modified measurement setup, where two identical lenses with 50 mm focal distance were used, one placed before the grating, and the other between the grating and the scanning plane to collimate the diffracted beams, which are needed to match those of a mixer array as described in the following paragraph. Using an integration similar to the 8-pixel grating case, we derive an efficiency of 66 ± 1%, where 2% uncertainty comes from the loss calculation of the lens. COMSOL simulation and the calculation in design predict power efficiencies to be 66.4% and 65%, respectively, which again show a good agreement to the experimental value.

To complete the study, we implement both gratings in a heterodyne experiment using a 2x2 HEB mixer array. We apply the 4-pixel grating together with the 1.4 THz gas laser to

Optics EXPRESS

optically pump the array. Since we have no 8-pixel mixer array available, we examine the 8-pixel grating by coupling three groups of four left, four centre or four right beams to the array. We succeeded in pumping all the mixers to reach their optimal (for the best sensitivity) operating current-voltage curves simultaneously. Applying the isothermal technique [19] to estimate the beam power at the detector and having estimated all the losses in the optical path from the laser to the mixer array and also taking the efficiency of the grating into account, we end up with about 25 μW for the total required input power, and about 50 μW for an 8-pixel mixer array. This order of power is reachable at lower frequencies (< 2 THz) by multiplier based solid state sources [13] and at higher frequencies by quantum cascade lasers [14].

4. Conclusion

We modelled and also experimentally demonstrated two Fourier phase gratings generating 2 × 2 and 2 × 4 beams from a single, coherent beam at 1.4 THz. Good agreements between the measurements and simulations are found for both the diffracted beam pattern and power efficiency. The measured efficiency is 66% for the 2x2 and 73% for the 2x4 grating, respectively. We also find that the incident angle can affect the distribution of power among the diffracted beams, but affects the efficiency negligibly. Furthermore, we confirm that the diffracted beams of the 4-pixel grating and 8-pixel grating are able to optically pump an array of superconducting HEB mixers. Thus, we demonstrate that the grating is an extremely promising technology for generating a multiple beam local oscillator for a heterodyne array at the supra-THz, required for future astronomic observatories, such as NASA Galactic-extragalactic ultra-long-duration spectroscopic stratospheric observatory (GUSTO).

Acknowledgments

One of the authors (B. M.) acknowledges the support and encouragement from Leo Kouwenhoven. The authors would also like to thank Matt Underhill for fabricating the gratings, David Thoen for helping with the surface profile measurements, and Paul Urbach and Akira Endo for their helps and useful discussions. TU Delft Space Institute is acknowledged for financial support.